Electronic Supplementary Material (ESI) for Journal of Materials Chemistry A.

Supplementary information

Rarely negative-thermovoltage cellulose ionogel with simultaneously boosting mechanical strength and ionic conductivity via ion-molecular engineering

Qunfeng Chen[1], Binbin Cheng[1], Zequn Wang[2], Xuhui Sun[2], Yang Liu[1], Haodong Sun[1], Jianwei Li[1], Lihui Chen[1], Xuhai Zhu[3], Liulian Huang[1], Yonghao Ni[1,4]*, Meng An[2]*,Jianguo Li[1]*

Methods

Materials

Bamboo cellulose is obtained from a dissolving pulp mill in Fujian Qingshan Paper Co., Ltd) (Sanming, China). 1-allyl-3-methylimidazolium chloride ([AMIM]Cl, ILs) was purchased from Lanzhou Yulu Fine Chemical Co., Ltd. (IL, Purity 99%, Lanzhou, China). Zinc chloride ($ZnCl_2$, 99.0%) was purchased from Shanghai Macklin Biochemical Co., Ltd. (Shanghai, China). Silver electrodes (thickness: 15 μm) were obtained from Zhongnuo Advanced Material (Beijing) Technology Co., Ltd. (Beijing, China).

Sample preparation

TEMPO-Mediated Oxidation of Cellulose： The bamboo pulp cellulose (5 g, net weight) was immersed in deionized water (100 mL), containing TEMPO (0.112 g) and NaBr (1.4 g), and the pH value was adjusted to ≈10.5 by adding 0.5 M NaOH solution. The NaClO (5 mmol) was slowly added to the solution to initiate the oxidation reaction. The pH of the solution was closely monitored using a pH meter and kept at a pH of 10.5. After 2 h, the reaction was terminated by adding 10 ml ethanol and 0.5 M HCl to adjust the pH to 7. Then the TEMPO-oxidized cellulose was collected and rinsed with deionized water several times.

Preparation of Cellulose Ionogels incorporating $ZnCl_2$ (CZ ionogel): Viscous homogeneous systems of cellulose/ILs with different dosages of $ZnCl_2$ were prepared by thermal dissolution at a constant temperature of 85°C. The content of ILs is ~60 wt.% and the concent of cellulose was 6 wt.%. The dosage of $ZnCl_2$ was 0.6 wt.%, 1.2

wt.%, 1.8 wt.%, and 2.4 wt.%. Extruding the cellulose/ILs homogeneous sample to a designated model, which was then bubble-free for 18 h in a vacuum oven at 85 °C. The CZ-x% ionogel was obtained following ten freezing-thawing cycles in the ultra-low temperature refrigerator at −80 °C and melting at room temperature to absorb water molecules, note that, the water content of the system is ~32 wt.%. Three hours were needed for freezing and one hour for melting As the control sample, cellulose ionogel (C ionogel) devoid of $ZnCl_2$ was used.

Characterizations

The surface functional groups were characterized by using FT-IR (Bruker VERTEX70, Karlsruhe, Germany) in the transmission mode with data recorded in the range of 600–4000 cm^{-1}. X-ray photoelectron spectroscopy (XPS) analysis was performed by an ESCALAB250XI electron spectrometer (Thermo Fisher Scientific, USA) with the energy resolution of 0.8 eV, binding energy scale was calibrated by C1s =284.8 eV, and its X source was a monochromatic Al target with an energy of 1486.6 eV. The morphologies of samples were obtained by using a field emission scanning electron microscope (FE-SEM, Zeiss Sigma 300) with a voltage of 5.00 kV equipped with energy-dispersive X-ray spectroscopy (EDS). The samples were gold-coated for 120 s after being freeze-dried as part of the preparation process. The storage and loss moduli (G′ and G″, respectively) of the samples were determined on a rotational rheometer (HAAKE, Germany) versus frequency and temperature. An ARLX'RA diffractometer with monochromatic Cu K radiation (k = 1.54056 Å) was used to conduct the X-ray powder diffraction analysis. The optical transmittance of the sample was detected by a

UV-Vis-NIR Spectrometer Lambda 750 (PerkinElmer, USA) at a 35 mm testing distance, with a wavelength range of 400–800 nm, in which the sample has a 4 mm thickness. Thermal gravimetric analysis (TGA) was performed on a thermogravimetric analyzer from 30 to 800 °C with a heating rate of 10 °C/min under the nitrogen atmosphere. The thermal properties were evaluated using differential scanning calorimetry (NETZSCH DSC 200 F3, Germany) at a heating or cooling rate of 10 °C/min after elimination of the thermal history under a nitrogen atmosphere with the temperature ranging from −150 °C to 200 °C. A tensile testing machine (KJ-1065B, China) was used to measure the tensile and compression properties of various materials at a speed of 10 mm min^{-1}. The bone-like sample has a width of 10 mm and thickness of 2 mm with more than 5 cm in length. The peak measured force was divided by the overlap area to yield the interfacial shear strength. The thermal conductivity of the ionogels with the size of 30×30×5 mm in the range of -20~60 °C was evaluated by a hotdisk (XIATECH TC3000E, China). The light-heat source for the light-induced thermoelectric generator comes from sunlight simulated by a Xenon lamp (PLS-SXE300, China).

Thermoelectric properties

The electrochemical performance of the samples was measured by an electrochemical workstation (CHI760, China). Electrochemical impedance spectroscopy (EIS) with voltage amplitude of 10 mV and frequency ranging from 100 kHz to 0.1 Hz, was used to measure the ionic conductivity I of samples. The sample (10 mm×5 mm×2 mm) was sandwiched between two electrodes. By extrapolating the curve with the abscissa based

on the equivalent circuit to the Nyquist plot as shown in Scheme S1, it was possible to determine the ionic intrinsic resistance of the samples. The ionic conductivities are calculated on the basis of the following equation 1.

$$\sigma_i = \frac{l}{RA} \tag{1}$$

Where σ_i is the ionic conductivity, l is the ionogel thickness, R is the resistance and A is the area. The thickness of ionogel was determined by a micrometer.

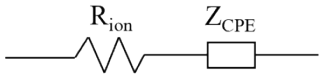

Scheme S1. Equivalent circuit for the analysis of the Nyquist plots.

Calculation of the dimensionless figure of merit (ZT_i)

The dimensionless figure of merit (ZT_i) of ionic thermoelectric (iTE) materials determines how effectively an ionic thermoelectric generator converts heat into electricity. The ZT_i values can be calculated by equation 2:

$$ZT_i = \frac{{\alpha_i}^2 \sigma_i}{k} T \tag{2}$$

where α_i is the ionic Seebeck coefficient, σ_i is the ionic conductivity, κ is the thermal conductivity, and T is the absolute temperature.

The ionic thermoelectric capacitor (iTE capacitor)

The ionogel was placed on the glass substrate with coated two Ag electrodes. As illustrated in Figure 5a, the iTE capacitor device was characterized to realize the practical application of heat-to-electricity through four-stage thermal cycling, similar to the previously reported method in the literature. Meanwhile, as shown in Figure S2, the capacitive property of the iTE capacitor was confirmed by the cyclic voltammetry

(CV) testing on an electrochemical workstation with a scan rate of 50 mV s^{-1}.

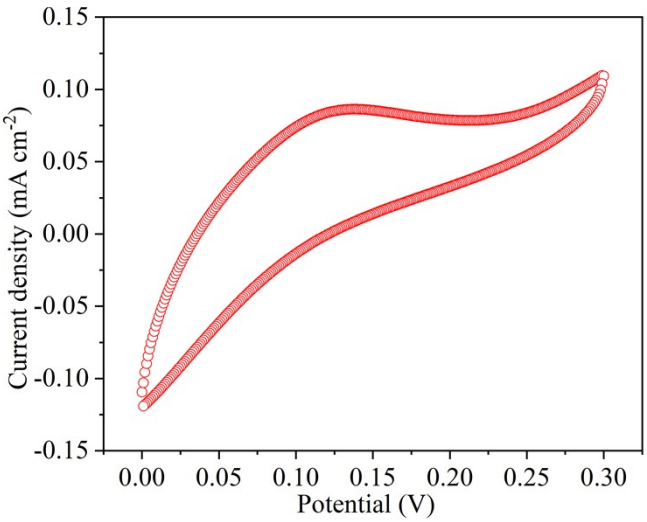

Figure S1. Cyclic voltammogram of an iTE capacitor with Ag electrode.

MD calculation of ionic diffusion

The potential energy of the systems *E* in our work is evaluated as a sum of individual energies (*Eq.* 3) for harmonic bond stretching and angle bending terms, Coulomb, and the 12-6 Lennard-Jones terms for the nonbonded interactions (*Eq.* 3-7).

$$E = E_{bonds} + E_{angles} + E_{nonbond} \tag{3}$$

$$E_{bonds} = \sum_{bonds} k_b \left(r - r_{eq}\right)^2 \tag{4}$$

$$E_{angles} = \sum_{angles} k_\theta \left(\theta - \theta_{eq}\right)^2 \tag{5}$$

$$E_{nonbond} = \sum_i \sum_{j>i} \left\{ \frac{q_i q_j e^2}{r_{ij}} + 4\varepsilon_{ij} \left[\left(\frac{\varepsilon_{ij}}{\sigma_{ij}} \right)^{12} - \left(\frac{\varepsilon_{ij}}{\sigma_{ij}} \right)^{6} \right] \right\} \tag{6}$$

where the parameters include the force constant k, the r_{eq}, θ_{eq}, indicate the equilibrium bond and angle values, partial atomic charges q, and Lennard-Jones well-

depths and radii, represented by ε and σ, respectively. The ε and σ used in *Eq.* 6 for the interaction of atom i and j is $\varepsilon_{ij} = \sqrt{\varepsilon_i \varepsilon_j}$ and $\sigma_{ij} = (\sigma_i + \sigma_j)/2$, respectively. We used LigParGen web-based service[1], which can obtain the OPLS force-field parameters and partial atomic charges for the cellulose chains and ILs. The TIP4P water model is adopted in our simulations. In our systems, all the atomic types in empirical potential are shown in Figure S2, and the non-bonded interaction parameters were listed in Table S1.

We generated a cellulose/ILs sample by placing cellulose chains, ILs, water molecules, Zn^{2+} cations and Cl^- anions in a cubic simulation box with a length of 7.0 nm using PACKMOL [2]. All MD simulations were performed and implemented by the large-scale atomic/molecular massively parallel simulator (LAMMPS) package[3]. The periodic boundary conditions were applied in all three directions. The cellulose/ILs sample was first equilibrated via the use of NPT-MD simulations at 300 K and 1 atm over a period of 0.5 ns until the temperature of the system, simulated box length and ILs mass density converge with time shown in Figures S3 and S4. Then, a further 0.5 ns simulation was performed in the NVT-MD. We tracked a trajectory of 1000 frames that were generated every 1 ps. Visual Molecular Dynamics (VMD)[4] was used to visualize the trajectories generated during simulations. The whole trajectory was then used for calculating the radial distribution function. The velocity Verlet algorithm with time step 0.1 fs was used to integrate Newton's equations of motion. The long-range interaction was calculated via the particle-particle particle-mesh (PPPM) approach with

an error parameter of 10^{-6}. The binding ability is evaluated using results from NVT-MD simulations. To achieve this, we first calculated the radial distribution function $g(r)$,

$$g(r) = \frac{n(r)}{\rho 4\pi r^2 \Delta r} \tag{7}$$

where the $n(r)$ represents the average number of particles in a spherical shell with a width of Δr at a distance r from the center reference particle, ρ is the average density of particles in the system.

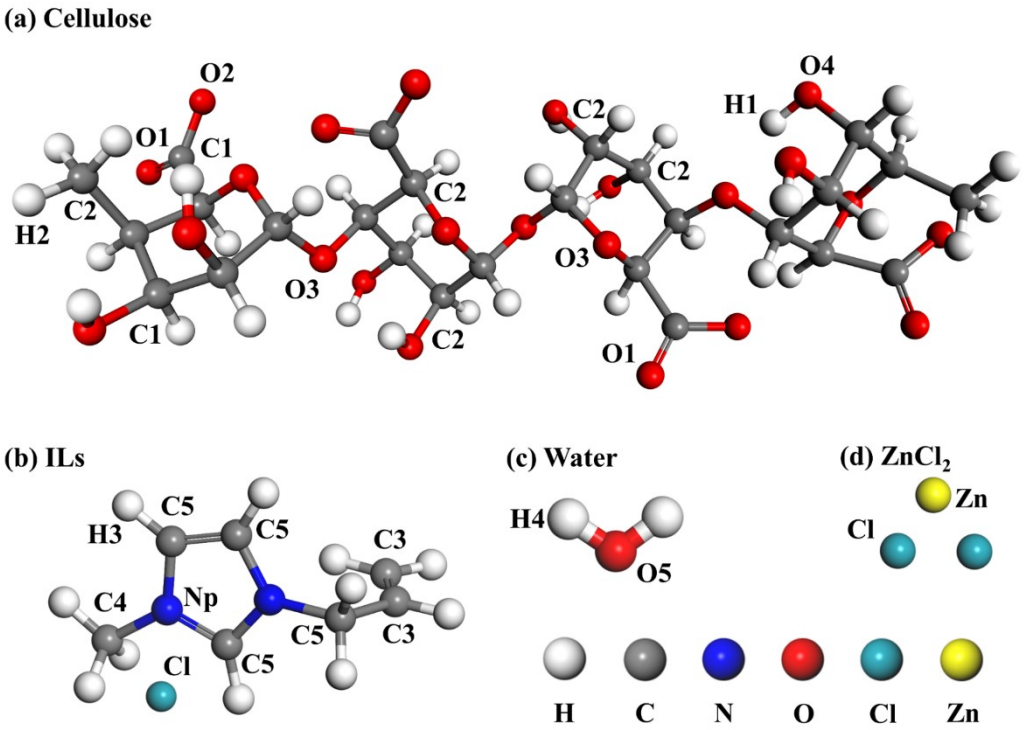

Figure S2. The atomic force field of cellulose/ILs sample in the MD simulations. (a) The atomic force field type of cellulose chains. (b) The atomic force field type of ILs. (c) The atomic force field type of water molecules. (d) The atomic force field type of Zn^{2+} and Cl^{-}.

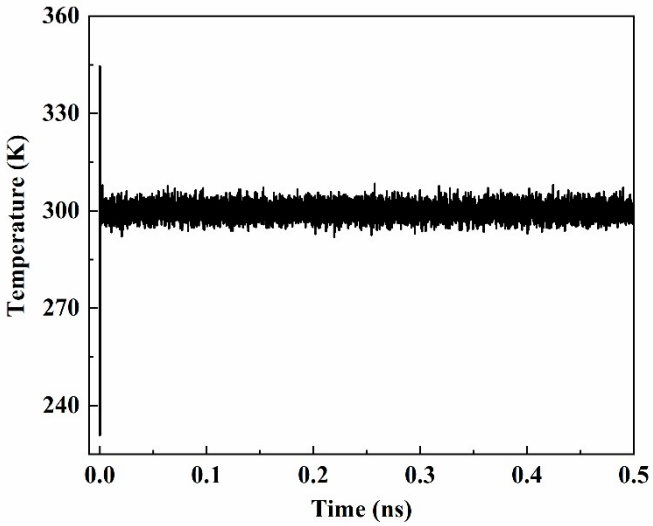

Figure S3. Evolution of system temperature over time during the NPT-MD stage, obtained from a Nose-Hoover thermostat.

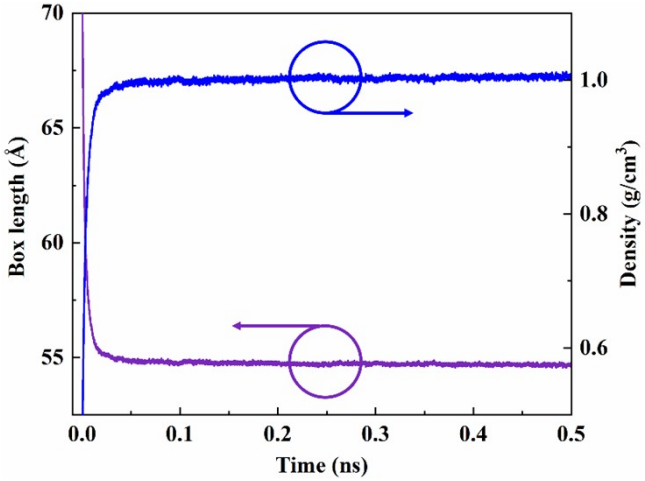

Figure S4. Evolution of the length of the simulation box and the mass density of ILs over time during the NPT-MD stage.

Table S1. The parameters in potential functions (VDW Parameter).

Atom type	ε (Kcal/mol)	σ (Å)
C1	0.0700	3.5500
C2	0.0660	3.5000
C3	0.0760	3.5000
C4	0.0660	3.5500
C5	0.0700	3.5500
Np	0.1700	3.2500
H1	0.0000	0.0000
H2	0.0300	2.5000
H3	0.0300	2.5000
H4	0.0000	0.0000
O1	0.1700	3.1200
O2	0.2100	2.9600
O3	0.1400	2.9000
O4	0.1700	3.1200
O5	0.1550	3.1536
Zn	0.2500	2.1800
Cl	0.1500	4.5400

Calculating binding energy

The binding energy is calculated by:

$$E_{binding} = E_{total} - (E_{chains} + E_{solute}) \tag{8}$$

where E_{total} is the energy after stabilization of a system comprising two chains and the solutes atom/molecule (Zn^{2+}, Cl^- and N+ ILs), E_{chains} and E_{solute} represent the system energy of two chains and solutes, respectively. The charge density of each chain was calculated based on the density functional theory using Vienna Ab initio Simulation Package (VASP)[20,21] along with the projector augmented wave (PAW) pseudopotentials. The Becke-Lee-Yang-Parr (BLYP) version of the generalized gradient approximation (GGA)[22] is used for the exchange-correction function. The convergence criteria for the total energy and ionic force were 1×10^{-8} eV and 0.02 eV·Å^{-1}, respectively. The cutoff energy of the plane-wave was set at 400 eV.

Figures and Tables

Table S2. The strength and conductivity of the CZ ionogel outperform many other ionogels with the 60 wt.% loading of ILs previously reported.

Materials	Tensile strength (MPa)	Conductivity (mS cm^{-1})	Ref
HPC/LA/AA/[Bmim]Cl	0.56	0.222	[12]
PVDF-HFP/EMIM：DCA	4.2	5.03	[10]
CNC/PIL/ EMIM[TFSI]	0.26	4.93	[6]
WPU/EMIM:DCA	0.6	12.6	[7]
PU/EMIM:DCA	1.61	15.36	[9]
Cellulose/[Bmim]Cl	3.5	38.5	[16]
TOBC/EMIM:DCA	1.2	47.63	[8]
BC/EMIM:DCA	3.05	32.97	[11]
BC/[Bmim]Cl	2.5	53.64	[18]
Cellulose/[AMIM]Cl	0.703	19.56	
This Work	4.46	67.43	

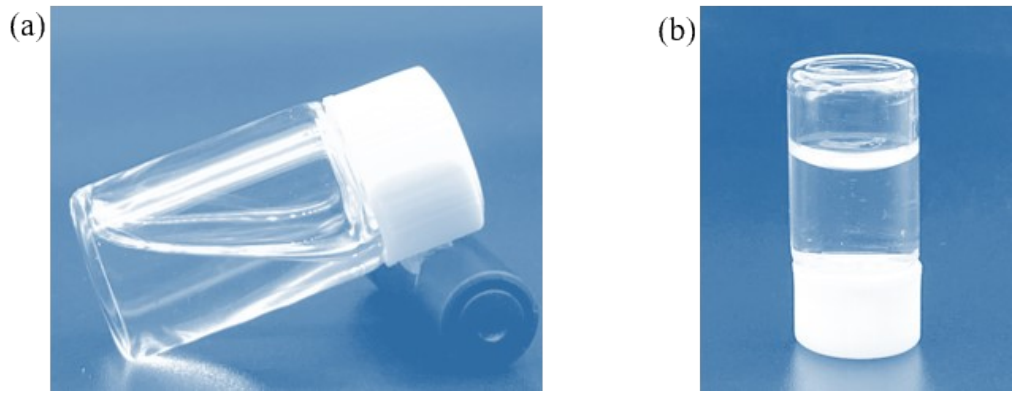

Figure S5. Photographs of the cellulose-$ZnCl_2$ solution a) and cellulose-$ZnCl_2$ ionogel b).

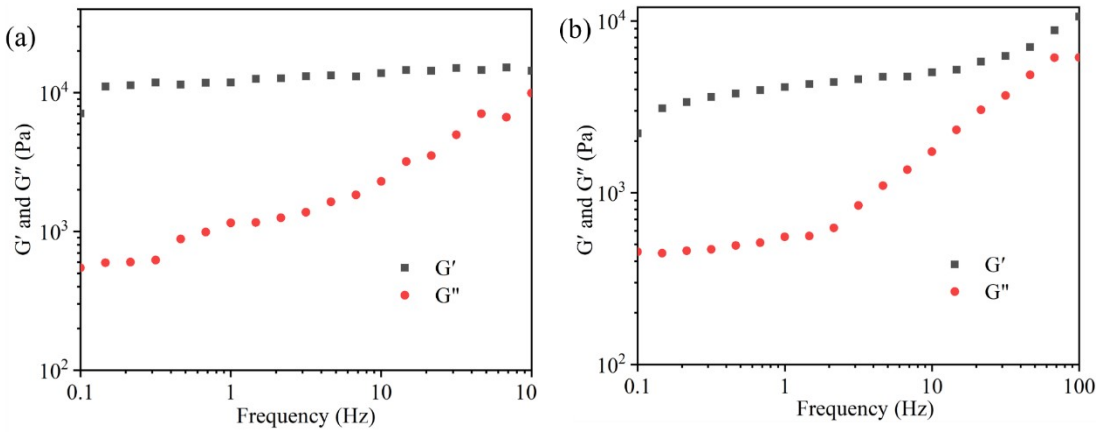

Figure S6. Variations of the storage modulus (G′) and loss modulus (G″) with the frequency, of the CZ ionogel (the dosage of $ZnCl_2$ is 1.2%) a) and C ionogel b).

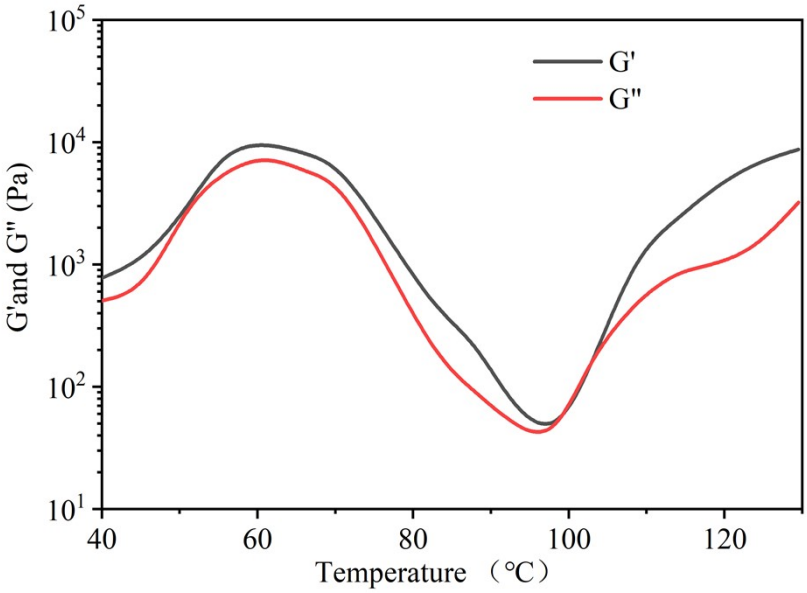

Figure S7. Variations of the storage modulus (G′) and loss modulus (G″) with the temperature of the CZ ionogel (the dosage of $ZnCl_2$ is 1.2%).

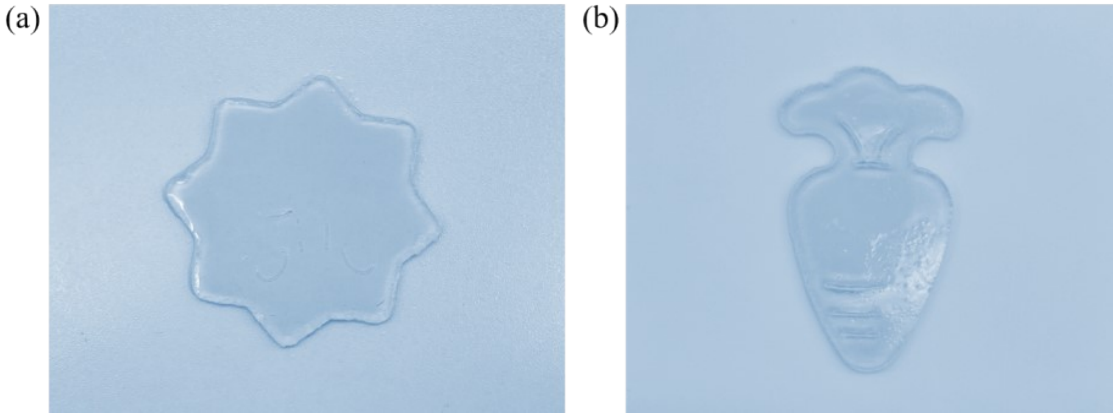

Figure S8. The customized CZ ionogels with the shapes of a star a) and a carrot b).

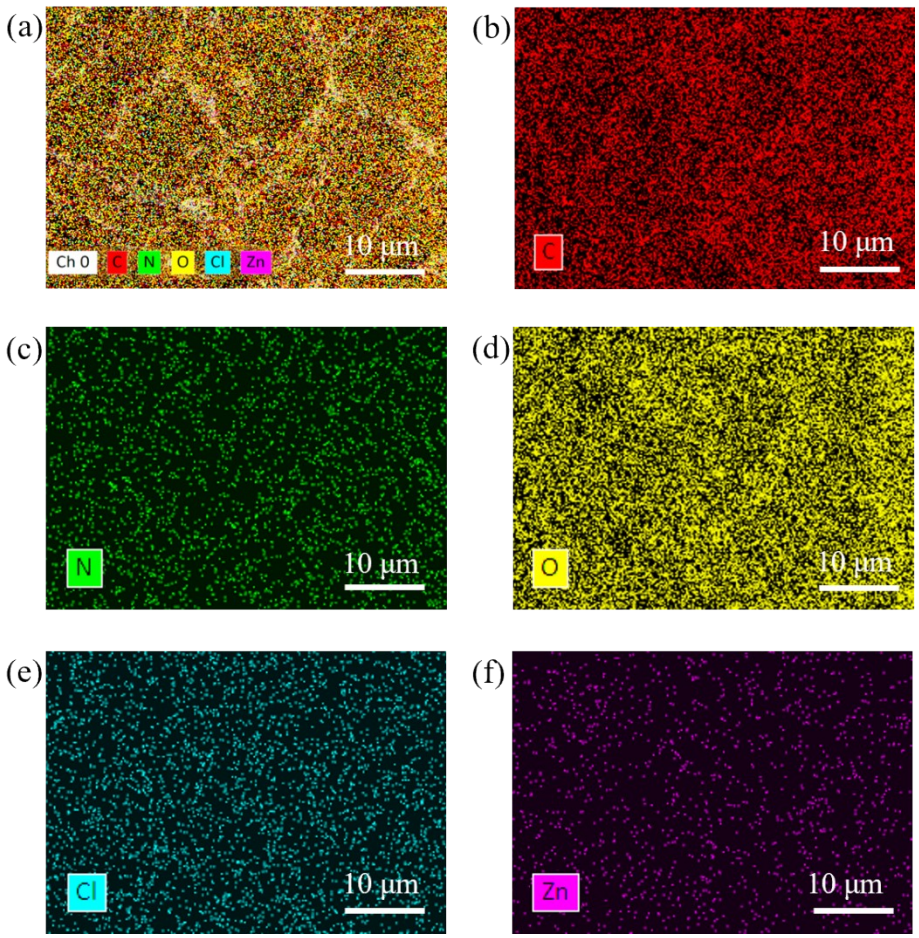

Figure S9. Elemental mapping of CZ-1.2% ionogel demonstrates the uniform distribution of ILs and $ZnCl_2$.

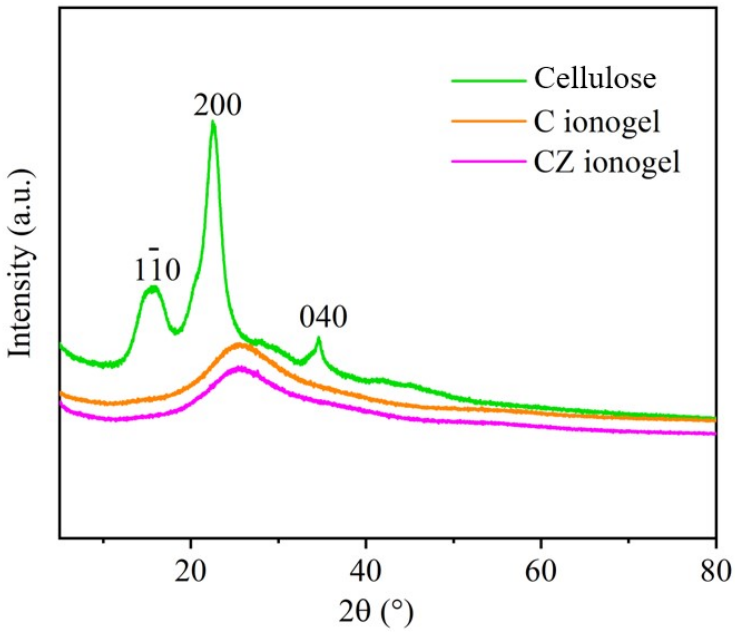

Figure S10. The XRD patterns of the cellulose, cellulose ionogel (C ionogel) and cellulose-$ZnCl_2$ ionogel (CZ ionogel).

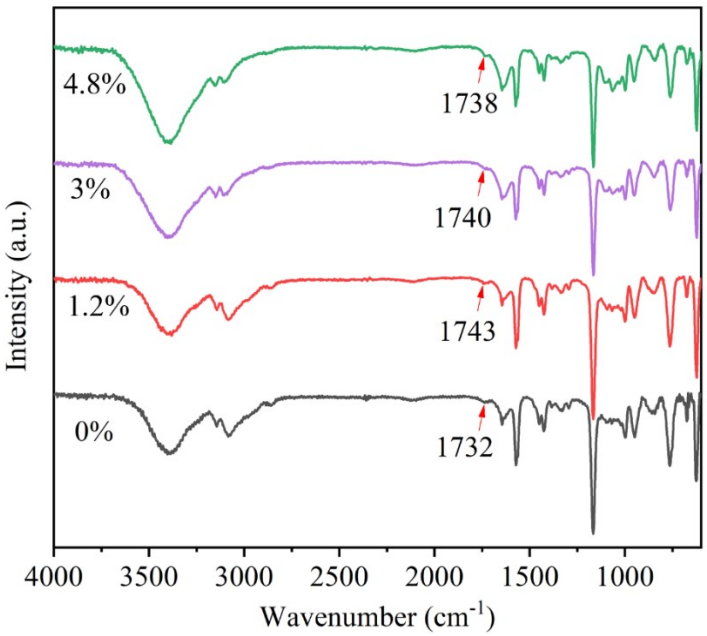

Figure S11. FT-IR spectra of the CZ ionogel with the $ZnCl_2$ dosage of 0%, 1.2%, 3%, and 4.8%.

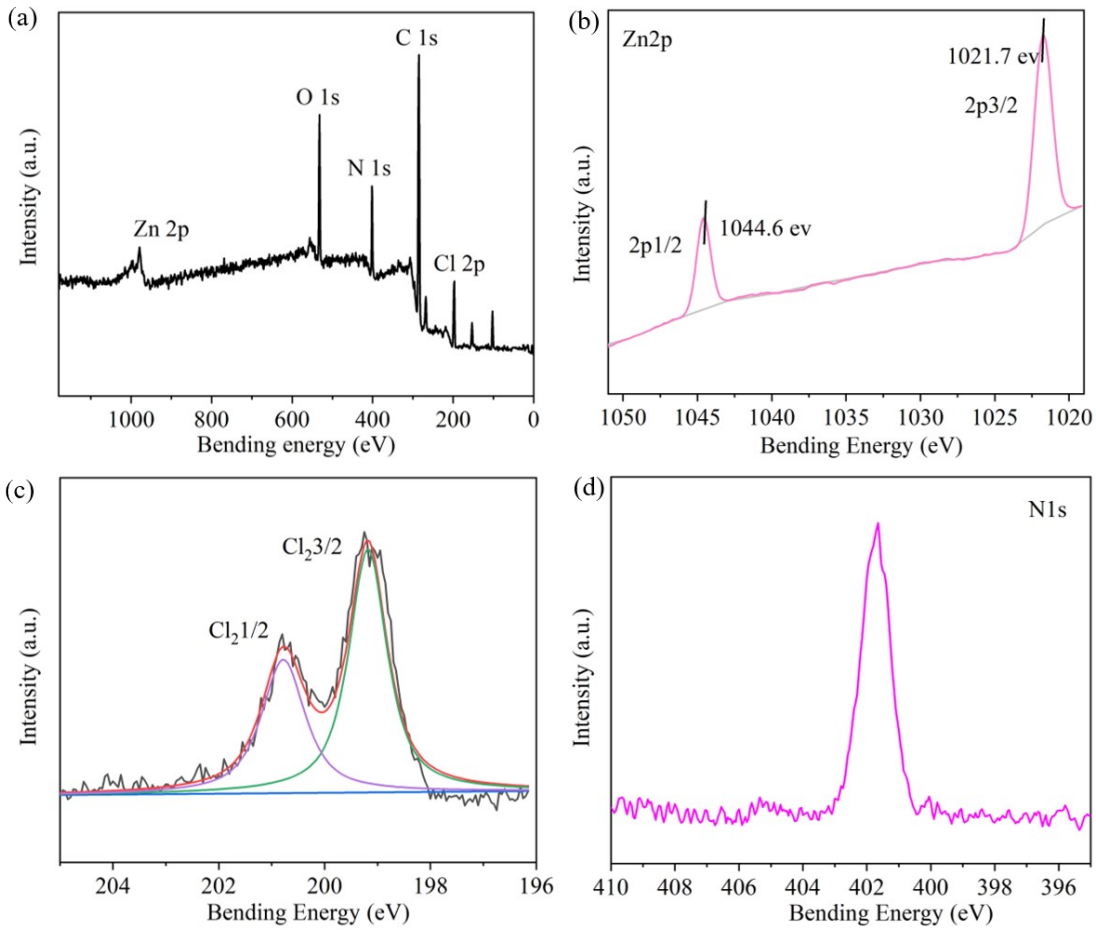

Figure S12. The XPS spectra of the CZ ionogel a), the element of Zn 2p b), and Cl 2p c) N 1s d) in the CZ ionogel (the dosage of $ZnCl_2$ is 1.2%).

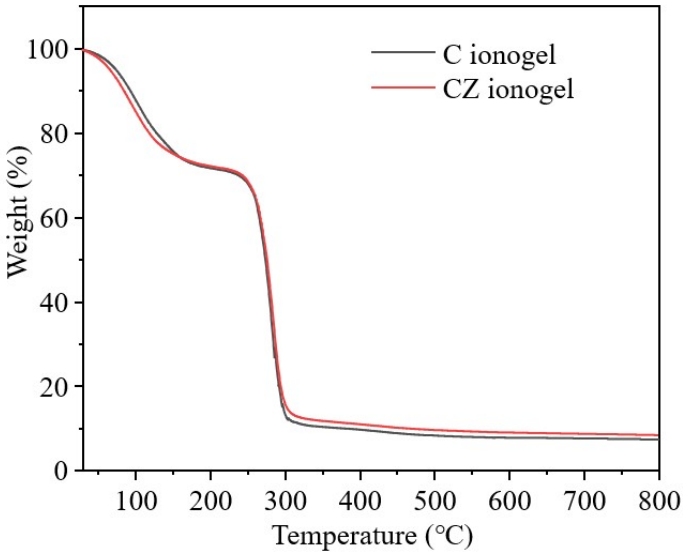

Figure S13. The results of TG for the C ionogel and the CZ ionogel (the dosage of $ZnCl_2$ is 1.2%).

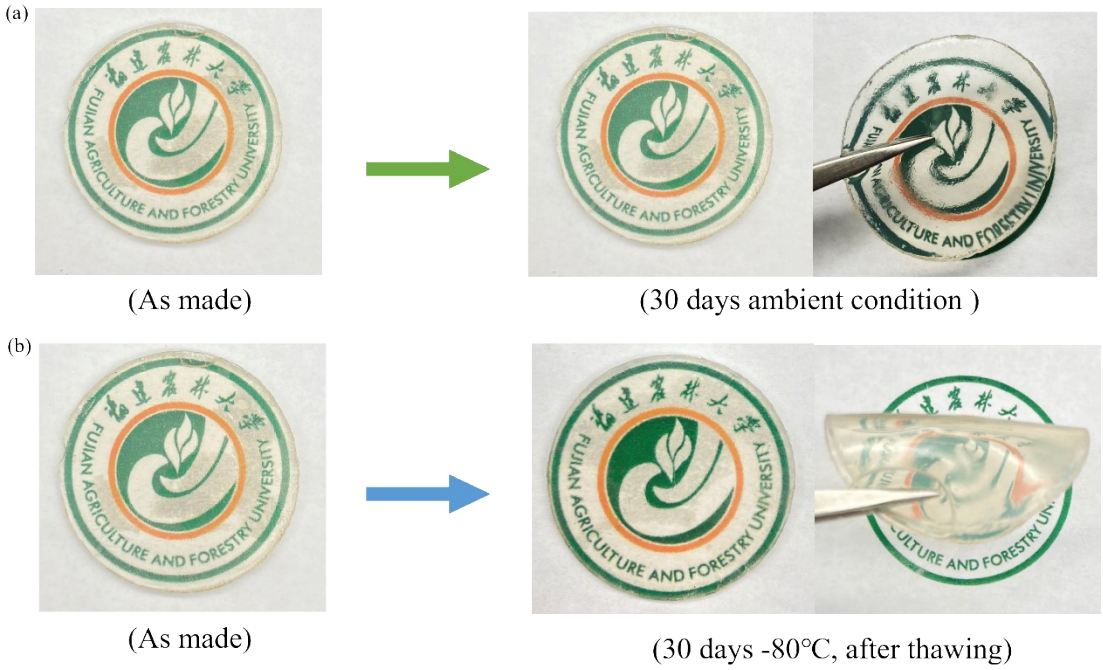

Figure S14. Comparison of the CZ ionogel (the dosage of $ZnCl_2$ is 1.2%) under ambient conditions a) and −80 °C b) for 30 days.

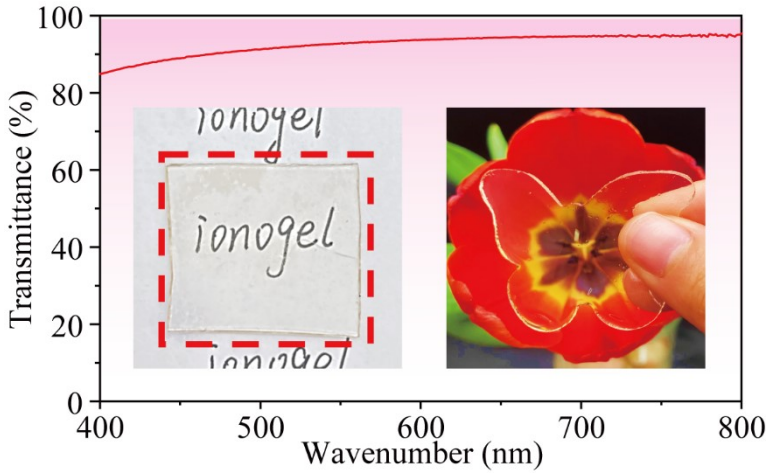

Figure S15. The CZ ionogel has an exceptional transmittance of up to 94% (the dosage of $ZnCl_2$ is 1.2%).

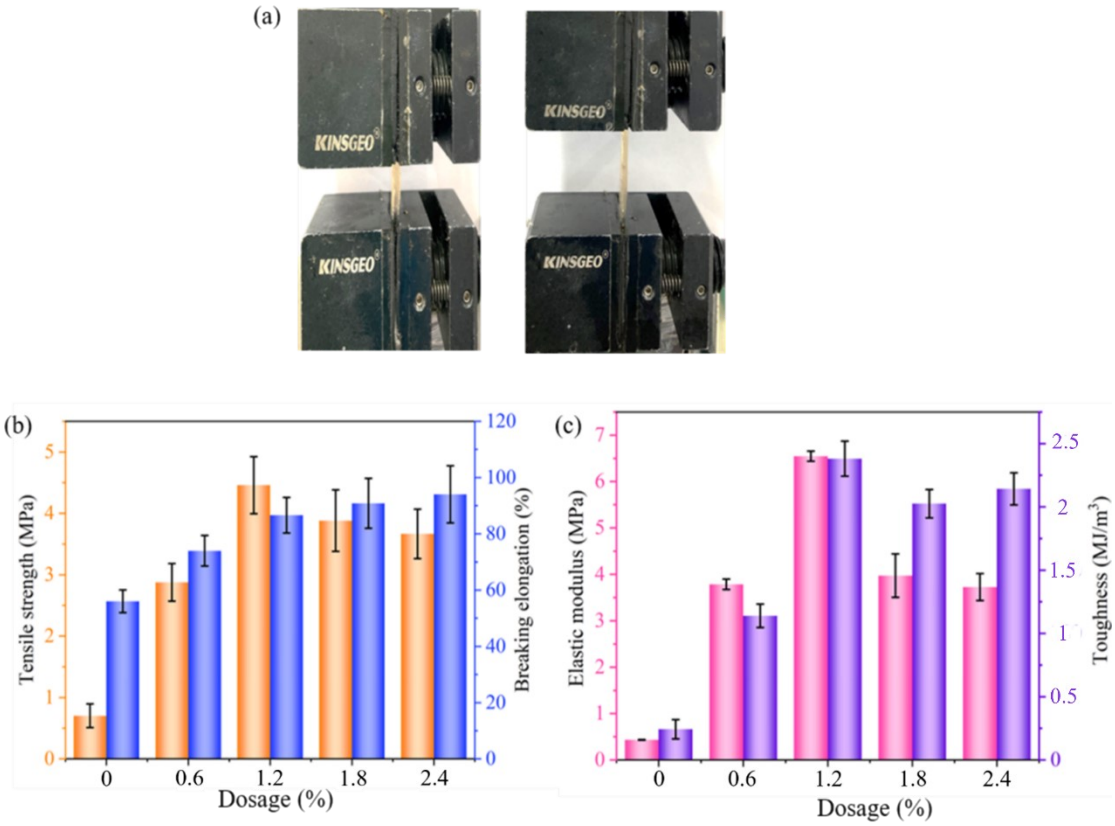

Figure S16. Digital photos of stretched ionogel a), tensile strength and breaking elongation of the ionogels with different dosages of $ZnCl_2$ b), and elastic modulus and toughness of the ionogels with different dosages of $ZnCl_2$ c).

Table S3. Comparison of the tensile strength and modulus of reference ionogels.

Materials	Tensile strength (MPa)	Modulus (MPa)	Ref.
PVC/DBA/[EMIM$^+$][TFSI$^-$]	0.06	0.00952	[5]
CNC/PIL/ EMIM[TFSI]	0.26	5.6	[6]
WPU/EMIM:DCA	0.6	0.63	[7]
TOBC/EMIM:DCA	1.2	1.12	[8]
PU/[PMIM$^+$][TFSI$^-$]	1.8	0.72	[9]
PVDF-HFP/EMIM：DCA	4.2	2	[10]
BC/EMIM:DCA	3.05	0.09	[11]
This Work	4.459	6.547	

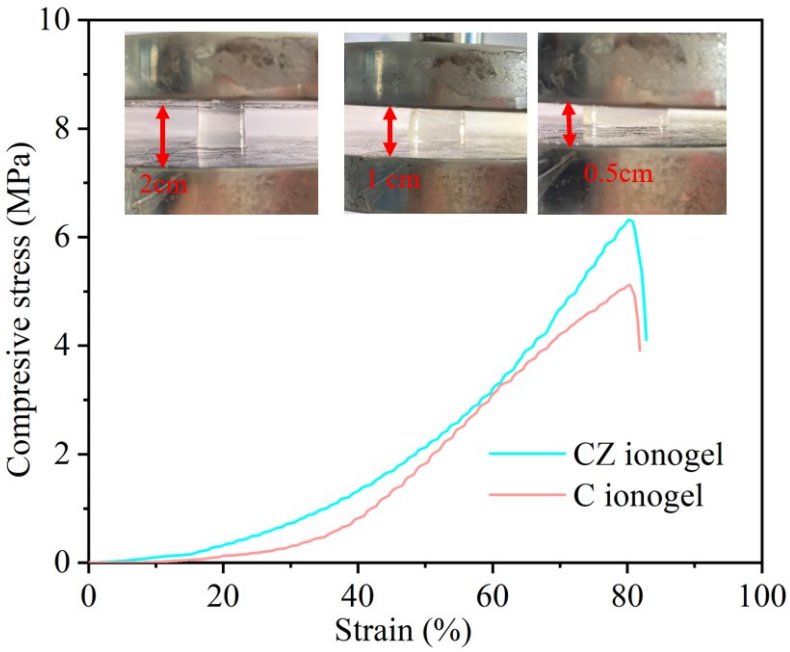

Figure S17. Compression process and compressive stress-strain curves of C and CZ ionogels (the dosage of $ZnCl_2$ is 1.2%).

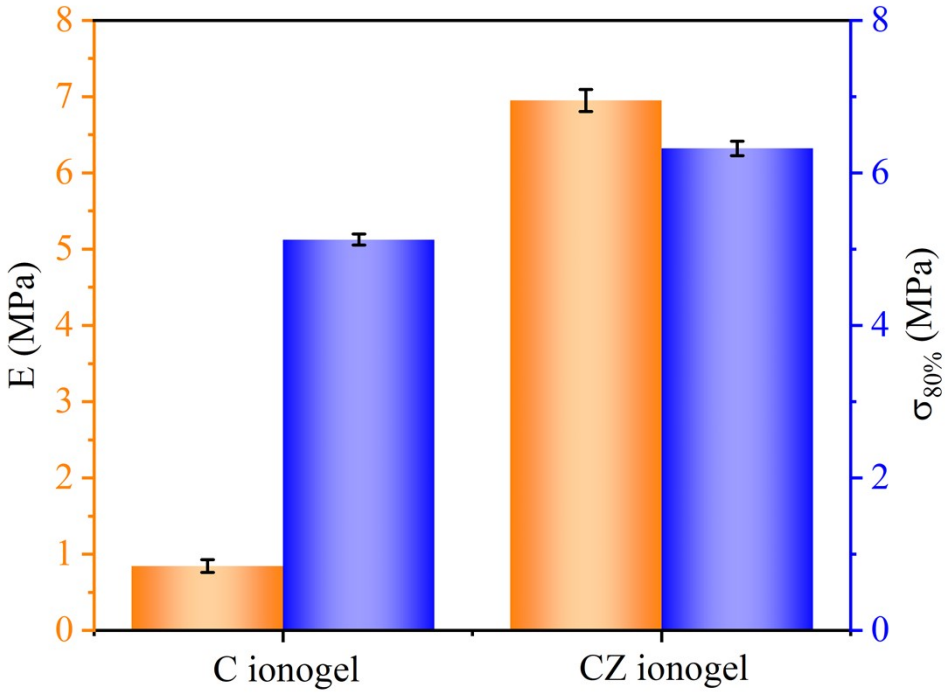

Figure S18. Compressive elastic modulus (E) and compressive strength at 80% strain of the C and the CZ ionogels (the dosage of $ZnCl_2$ is 1.2%).

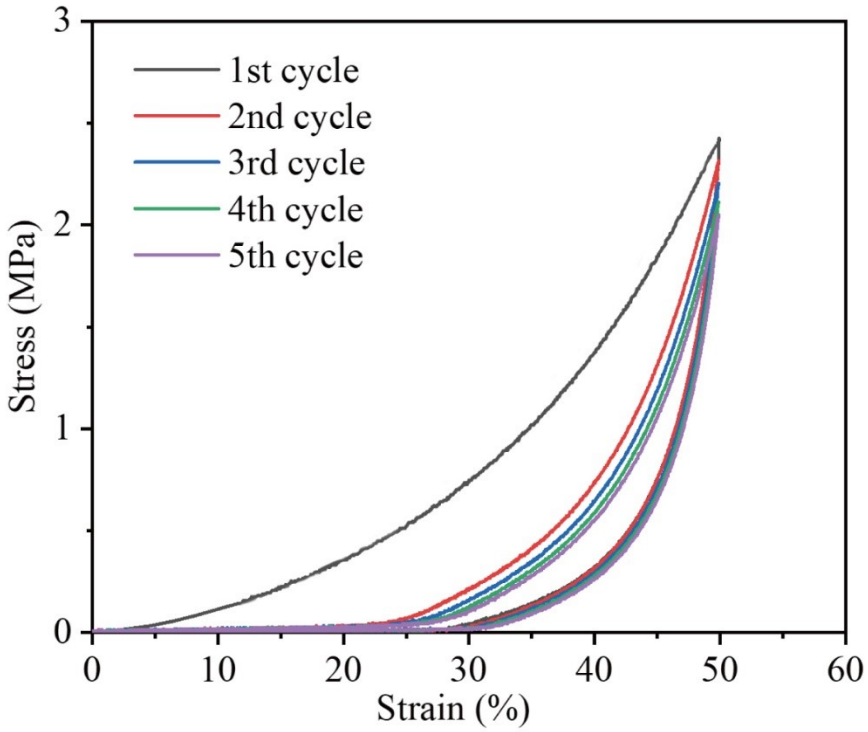

Figure S19. Cyclic compressive stress-strain curves of the CZ ionogel with a maximum strain of 50% (the dosage of $ZnCl_2$ is 1.2%).

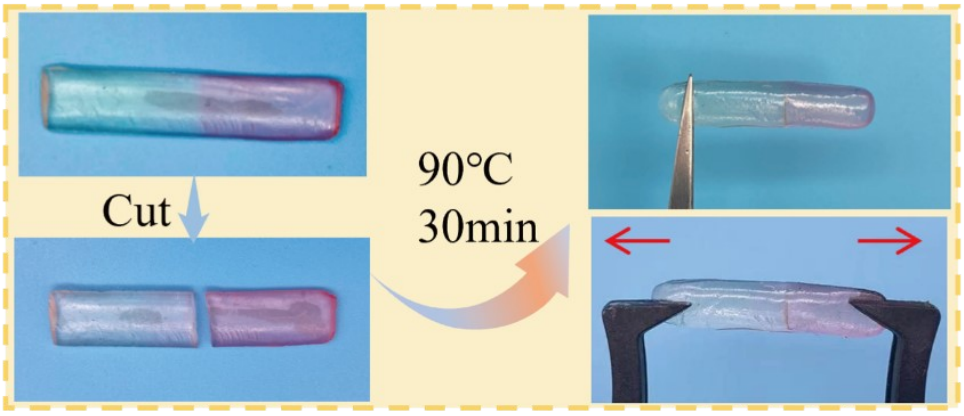

Figure S20. Self-healing properties of the CZ ionogel. The cut CZ ionogel can be healed by heating at 90 ℃ for 30 min (the dosage of $ZnCl_2$ is 1.2%).

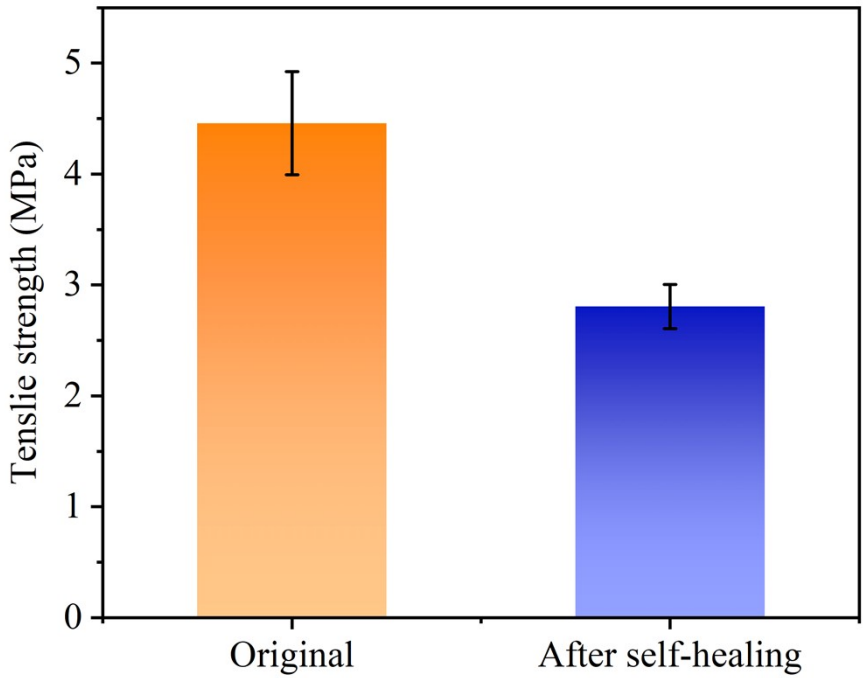

Figure S21. Comparison of tensile strength of the CZ ionogel before and after self-healing (the dosage of $ZnCl_2$ is 1.2%).

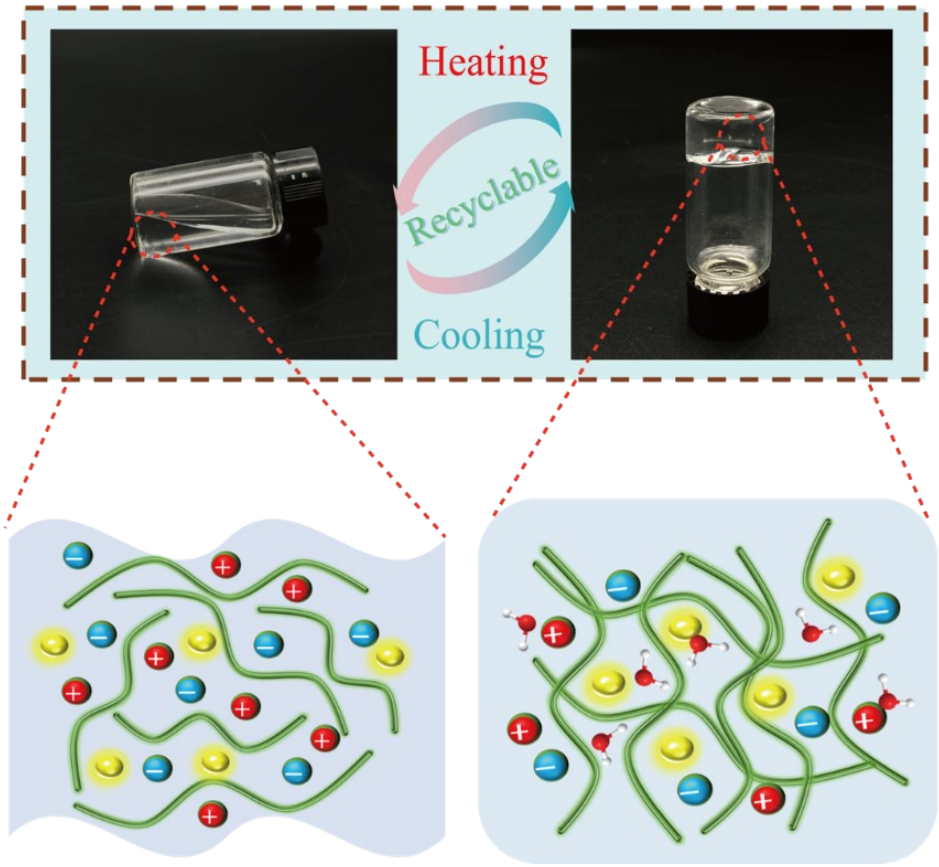

Figure S22. The CZ ionogel can be heated and cooled to achieve its reconstruction and recycling (the dosage of $ZnCl_2$ is 1.2%).

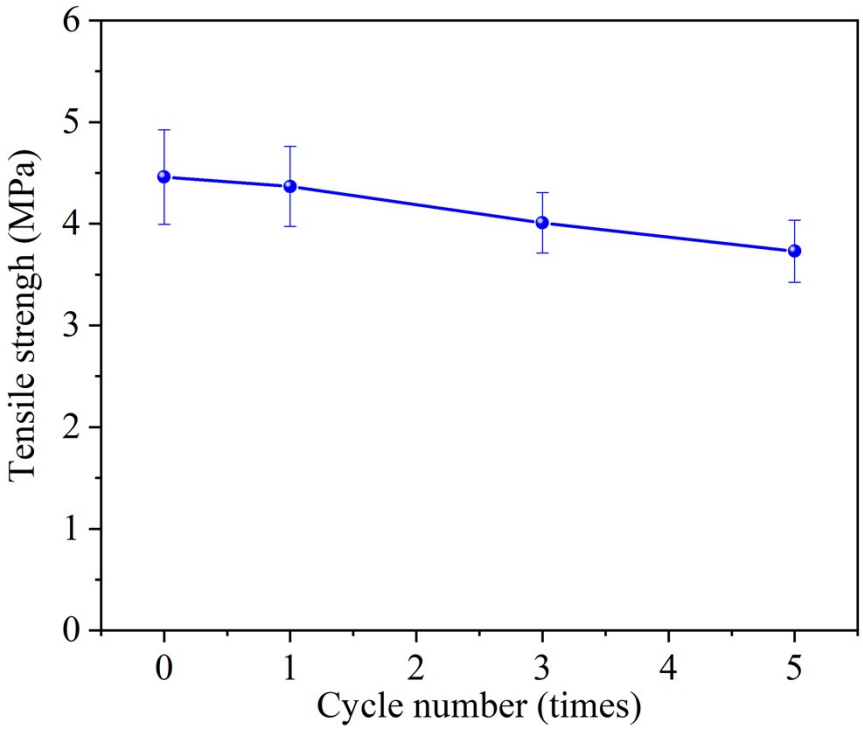

Figure S23. The tensile strength of CZ ionogel varies with the number of cycles (the dosage of $ZnCl_2$ is 1.2%).

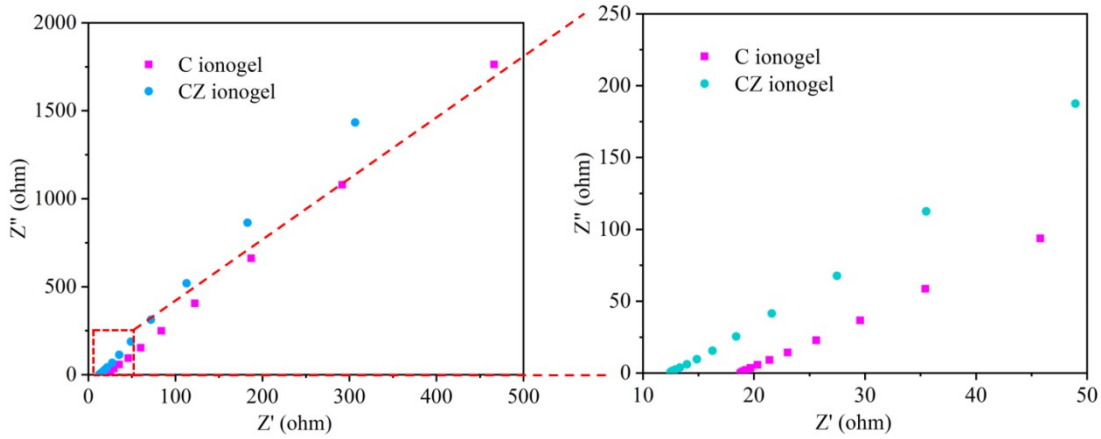

Figure S24. Nyquist plots of the C ionogel and CZ ionogel at 20 °C and the amplification in the low impedance range (the dosage of $ZnCl_2$ is 1.2%).

Table S4. Comparison of the conductivity of reference ionogels.

Materials	Conductivity (mS cm^{-1})	Ref
HPC/LA/AA/[Bmim]Cl	0.074	[12]
PIL-PEI	1.03	[13]
SP-DN/ILs	1.94	[14]
TMPTMA	6.15	[15]
PVDF-HFP/EMIM：DCA	6.7	[10]
CNC/PIL/ EMIM[TFSI]	7.8	[6]
WPU/EMIM:DCA	11.7	[7]
PU/EMIM:DCA	12.8	[9]
[BMIM][BF4]/PDMAA	22.1	[16]
Cellulose/[Bmim]Cl	38.5	[17]
SiO_2/EMIM:DCA	47.5	[18]
BC/EMIM:DCA	54.6	[11]
BC/[Bmim]Cl	62.58	[19]
This Work	67.43	

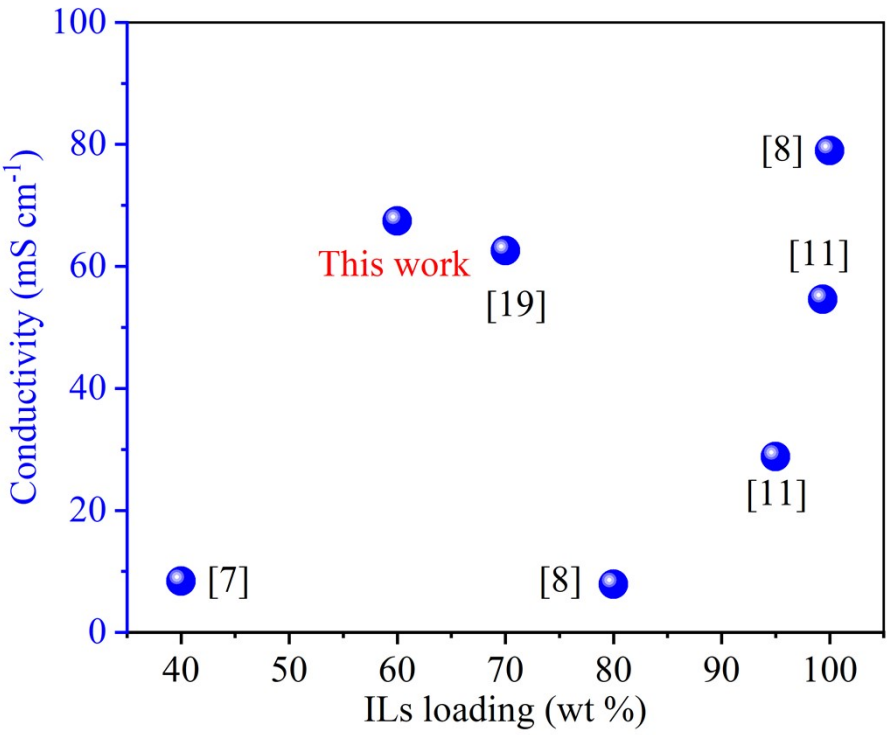

Figure S25. The evaluation of reference ionogel conductivity under various ILs loading.

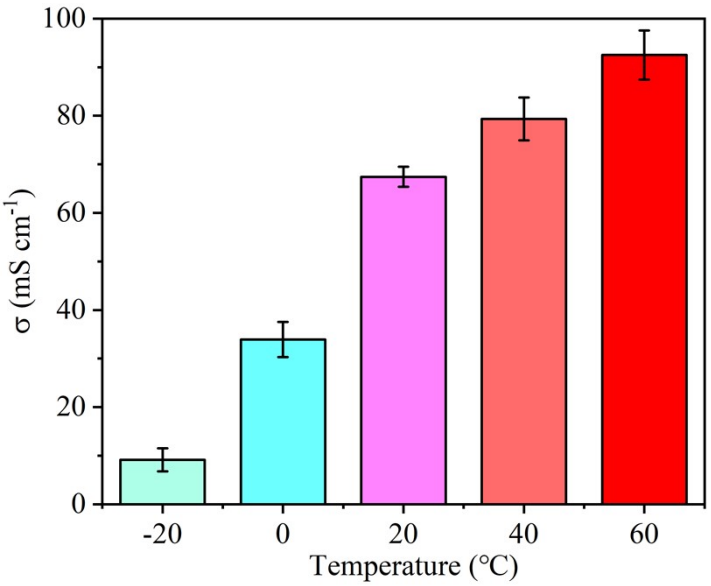

Figure S26. The conductivity of the CZ ionogel at various temperatures (the dosage of $ZnCl_2$ is 1.2%).

Table S5. The mass density of both pure ILs and ILs in the MD model of CZ ionogel at room temperature.

System	Mass density (g/cm^3)
Pure ILs	1.16
ILs in the MD model	1.01

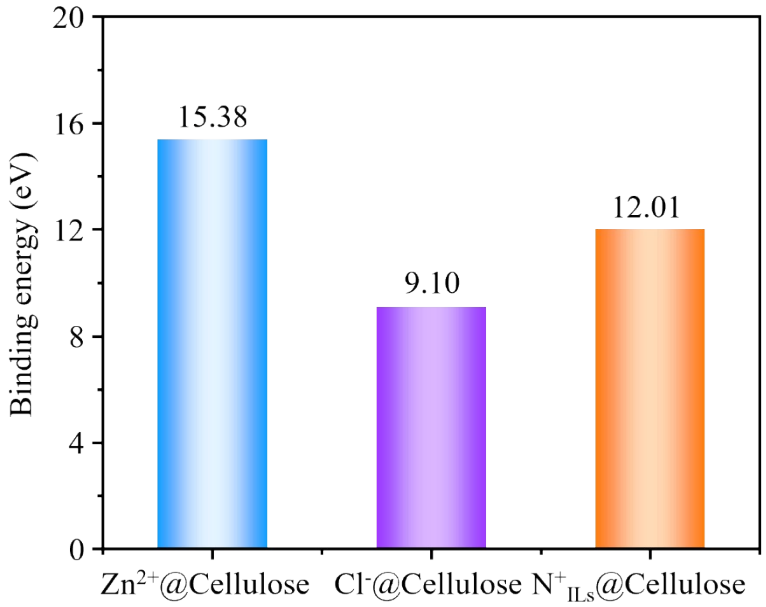

Figure S27. The binding energy between oxygen species of side group in cellulose and Zn^{2+}, Cl^{-}, N+ ILs ions.

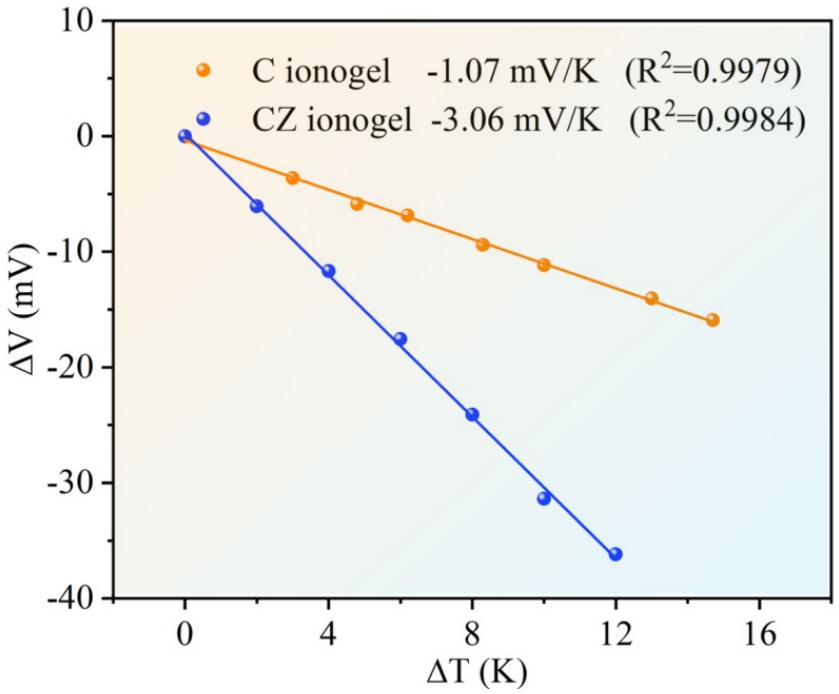

Figure S28. Linear fitting of ionic Seebeck coefficients of the C ionogel and the CZ ionogel (the dosage of $ZnCl_2$ is 1.2%).

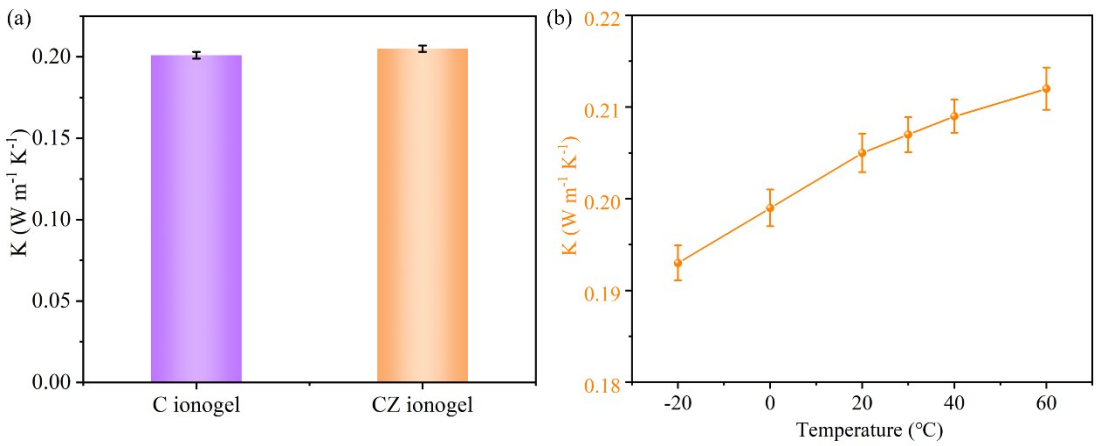

Figure S29. Thermal conductivity of C and CZ ionogels (the dosage of $ZnCl_2$ is 1.2%) at 30 °C a) and the thermal conductivity of the CZ ionogels (the dosage of $ZnCl_2$ is 1.2%) as a function of temperature b).

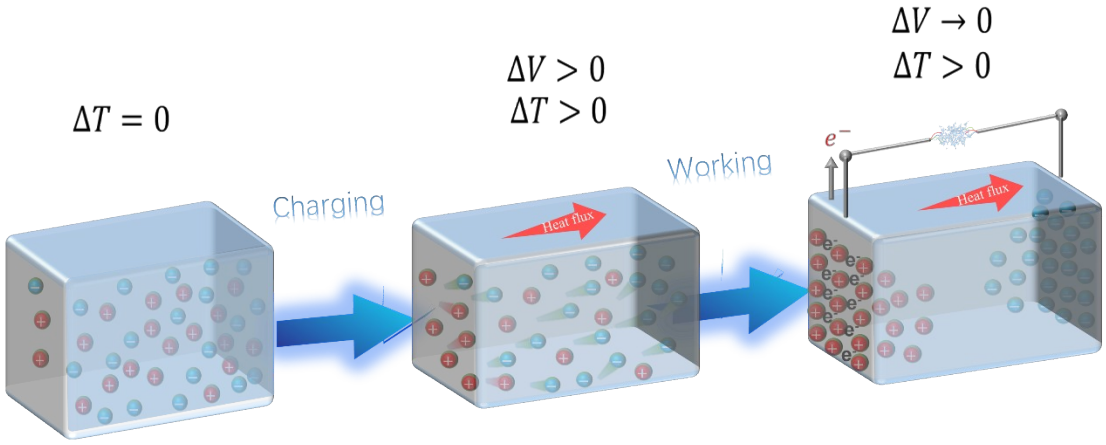

Figure S30. Schematic diagram of the working principle of iTE material as a capacitor.

References

[1] L. S. Dodda, I. C. Vaca, J. Tirado-Rives, W. L. Jorgensen, *Nucleic Acids Res.* W1 **2017**, 45, W331-W336.

[2] L. Martínez, R. Andrade, E. G. Birgin, J. M. Martínez, *J. Comput. Chem.* **2009**, 30, 2157-2164.

[3] S. Plimpton, *J. Comput. Phys.* **1995**, 117, 1-19.

[4] W. Humphrey, A. Dalke, K. Schulten, *Journal of molecular graphics,* **1996**, 14, 33-38.

[5] Y. J. Son, S. Seo, K. Y. Chun, J. W. Bae, H. J. Lee, S. Bae, S. Baik, C. S. Han, *Sensor. Actuat. A-Phys.* **2022**, 113328.

[6] H. Lee, A. Erwin, M. L. Buxton, M. Kim, A. V. Stryutsky, V. V. Shevchenko, A. P. Sokolov, V. V. Tsukruk, Shape Persistent, *Adv. Funct. Mater.* **2021**, 31, 2103083.

[7] Y. Fang, H. Cheng, H. He, S. Wang, J. Li, S. Yue, L. Zhang, Z. Du, J. Ouyang, *Adv. Funct. Mater.* **2020**, 30, 2004699.

[8] G. Fan, K. Liu, H. Su, Y. Luo, Y. Geng, L. Chen, B. Wang, Z. Mao, X. Sui, X. Feng, *Chem. Eng. J.* **2022**, 434, 134702.

[9] J. Xu, H. Wang , X. Du, X. Cheng, Z. Du, H. Wang, *ACS Appl. Mater. Inter.* **2021**, 13, 20427−20434.

[10] H. Cheng, X. He, Z. Fan, J. Ouyang, *Adv. Energy Mater.* **2019**, 9, 1901085.

[11] K. Liu, J. Lv, G. Fan, B. Wang, Z. Mao, X. Sui, X. Feng, *Adv. Funct. Mater.* **2022**, 32, 2107105.

[12] C. Dang, C. Shao, H. Liu, Y. Chen, H. Qi, *Nano Energy,* **2021**, 106619.

[13] L. Liang, W. Yuan, X. Chen, H. Liao, *Chem. Eng. J.* **2021**, 421,130000.

[14] Y. Liang, K. Wang, J. Li, H. Wang, X. Xie, Y. Cui, Y. Zhang, M. Wang, C. Liu, *Adv. Funct. Mater.* **2021**, 31, 2104963.

[15] Q.Wang, P. Zhang, B. Wang, L. Fan, *Electrochim. Acta,* **2021**, 370, 137706.

[16] X. Liu, O. O. Taiwo, C. Yin, M. Ouyang, R. Chowdhury, B. Wang, H. Wang, B. Wu, N. P. Brandon, Q. Wang, S. J. Cooper, *Adv. Sci.* **2019**, 6, 1801337.

[17] D. Zhao, Y. Zhu, W. Cheng, G. Xu, Q. Wang, S. Liu, J. Li, C. Chen, H. Yu, L. Hu, *Matter,* **2020**, 2, 390-403.

[18] X. He, H. Cheng, S. Yue, J. Ouyang, *J. Mate.r Chem. A* **2020**, 10813–10821.

[19] G. Jiang, G. Wang, Y. Zhu, W. Cheng, K. Cao, G. Xu, D. Zhao, H. Yu, *Research,* **2022**, 9814767.

[20] G. Kresse, J. Furthmüller, *Phy. Review B*, **1996**, 54(16): 11169.

[21] G. Kresse, D. Joubert, *Phy. Review B*, **1999**, 59(3): 1758.

[22] P. M. Gill, B. G. Johnson, J. A. Pople, *Chemical Physics Letters*, **1992**, 197(4-5): 499-505.